



# Segment Membranes and Nuclei from Histopathological Images via Nuclei Point-Level Supervision

Hansheng Li<sup>1</sup>, Zhengyang Xu<sup>1</sup>, Mo Zhou<sup>1</sup>, Xiaoshuang Shi<sup>2</sup>, Yuxin Kang<sup>1</sup>, Qirong Bu<sup>1</sup>, Hong Lv<sup>3</sup>, Ming Li<sup>3</sup>, Mingzhen Lin<sup>4</sup>, Lei Cui<sup>1(✉)</sup>, Jun Feng<sup>1</sup>, Wentao Yang<sup>3</sup>, and Lin Yang<sup>1</sup>

<sup>1</sup> Northwest University, Xi'an, China

leicui@nwu.edu.cn

<sup>2</sup> University of Electronic Science and Technology, Chengdu, China

<sup>3</sup> Fudan University, Shanghai, China

<sup>4</sup> Shanghai Second Medical University, Shanghai, China

**Abstract.** Accurate segmentation and analysis of membranes from immunohistochemical (IHC) images are crucial for cancer diagnosis and prognosis. Although several fully-supervised deep learning methods for membrane segmentation from IHC images have been proposed recently, the high demand for pixel-level annotations makes this process time-consuming and labor-intensive. To overcome this issue, we propose a novel deep framework for membrane segmentation that utilizes nuclei point-level supervision. Our framework consists of two networks: a Seg-Net that generates segmentation results for membranes and nuclei, and a Tran-Net that transforms the segmentation into semantic points. In this way, the accuracy of the semantic points is closely related to the segmentation quality. Thus, the inconsistency between the semantic points and the point annotations can be used as effective supervision for cell segmentation. We evaluated the proposed method on two IHC membrane-stained datasets and achieved an 81.36% IoU and 85.51%  $F_1$  score of the fully supervised method. *All source codes are available [here](#).*

**Keywords:** Membrane segmentation · Point-based supervision · Immunohistochemical image

## 1 Introduction

Accurate quantification of immunohistochemistry (IHC) membrane staining images is a crucial aspect of disease assessment [14, 15]. In clinical diagnosis, pathologists typically grade diseases by manually estimating the proportion of stained membrane area [14] or evaluating the completeness of stained membrane [23]. However, this manual

L. Cui, J. Feng, W. Yang and L. Yang—Equally contribution.

H. Li and Z. Xu—Equally first authors.

**Supplementary Information** The online version contains supplementary material available at [https://doi.org/10.1007/978-3-031-43987-2\\_52](https://doi.org/10.1007/978-3-031-43987-2_52).

approach is tedious, time-consuming [22], and error-prone [13]. Therefore, there is an urgent need for precise automatic IHC membrane analysis methods to provide objective quantitative evidence and improve diagnostic efficiency.

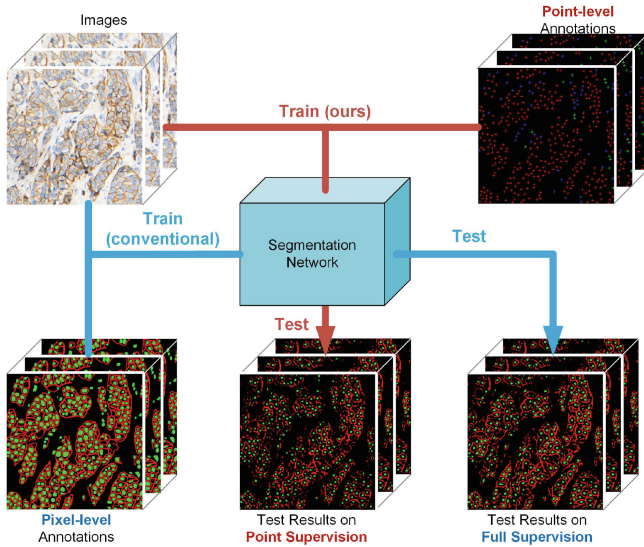


**Fig. 1.** Illustration of the full supervision (blue line) and point supervision (ours, red line) for membranes and nuclei segmentation. (Color figure online)

Despite numerous deep learning methods have been proposed for detecting cell nuclei [11,20] from hematoxylin-eosin (H&E) staining images, little attention has focused on analyzing cell membranes from IHC images. Currently, only a few fully supervised IHC membrane segmentation methods have been proposed [9,19], demonstrating the superiority of deep learning-based membrane segmentation. However, full supervision requires substantial time and effort for pixel-level annotations of cell membranes and nuclei. In contrast, as annotating the centers of nuclei requires much fewer efforts, weakly supervised learning has been studied for nuclei segmentation [16,21]. Nevertheless, how to utilize point annotations to supervise cell membrane segmentation is still under investigation.

This study proposes a novel point-based cell membrane segmentation method, which can significantly reduce the cost of pixel-level annotation required in conventional methods, as shown in Fig. 1. In this study, the category of the point annotation is used to describe the staining state of the cell membrane (e.g., complete-stained, incomplete-stained, and unstained). We employ a network named Seg-Net to segment the nuclei and membranes separately, followed by a Trans-Net to convert the segmentation results into semantic points. Since the accuracy of semantic points is directly related to the segmentation results, the segmentation quality can be implicitly supervised by the loss between the semantic points and the point annotations, as shown in Fig. 2.

To the best of our knowledge, this is the first study that using point-level supervision for membrane segmentation from IHC images, which could significantly advance future

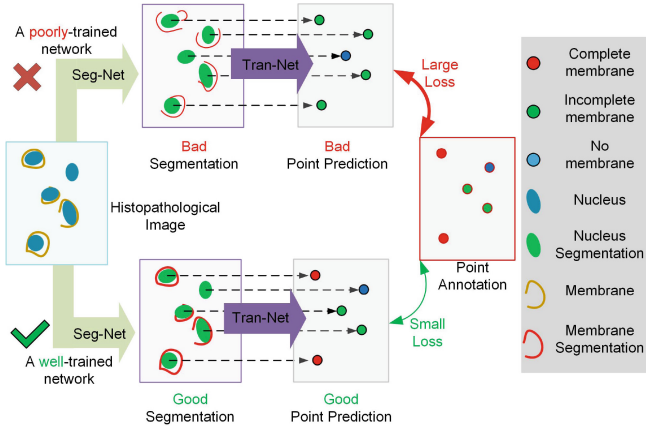


**Fig. 2.** The illustration of how point annotations are used to supervise the cell segmentation.

membrane analysis. Additionally, our method is the first to employ point annotations to simultaneously supervise the segmentation of two objects. Extensive experiments confirm the efficacy of the proposed method, attaining performance that is comparable to models trained with fully supervised data.

## 2 Related Works

Deep learning-based segmentation methods have been widely developed for cell nuclei segmentation from H&E images in recent years, ranging from convolutional neural networks [5, 12, 24] to Transformer-based architectures [8], resulting in continuously improved accuracy in nuclei segmentation.

For the task of analyzing IHC membrane-stained images, due to the challenge of pixel-level annotation, existing methods mostly adopt traditional unsupervised algorithms, such as watershed [17, 26], active contour [3, 25], and color deconvolution [2, 4]. These traditional methods perform inadequately and are vulnerable to the effects of differences in staining intensity and abnormal staining impurities. In recent years, a few fully supervised cell membrane segmentation methods also have emerged [9, 19], but the high cost of data annotation limits their applicability to various membrane staining image analysis tasks.

To reduce the annotation cost of nuclei segmentation in histopathological images, weakly supervised segmentation training methods have received attention, including: 1) Unsupervised cell nuclei segmentation methods represented by adversarial-based methods [6, 7]. However, unsupervised methods are challenged by the difficulty of constraining the search space of model parameters, making it hard for the model to handle visually complex pathology images, such as H&E or IHC; 2) Weakly supervised cell nucleus segmentation algorithms with point annotation [16, 21]. Because the cell nucleus shape in H&E images is almost elliptical, point annotation combined with

Voronoi diagram [1] were used to generate pseudo-annotations for iterative model training and refinement. Although these methods can perform weakly supervised segmentation of cell nuclei from IHC membrane-stained images, they are usually ineffective in segmenting messy cell membranes.

Therefore, this paper proposes a novel point-supervised cell membrane segmentation method, addressing a major challenge in the field. The paper also explores the feasibility of point supervision for the segmentation of two types of objects (cell nuclei and cell membranes) for the first time.

### 3 Method

This study aims to explore how to perform membrane and nucleus segmentation in IHC membrane-stained images using only point-level supervision. Nuclei segmentation is performed for cell localization and counting, while membrane quantification provides clinical evidence for diagnosis.

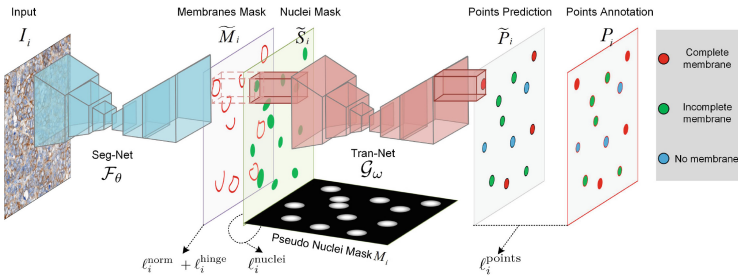


**Fig. 3. The architecture of the proposed framework.** The training stage employs two networks, namely a Segmentation network (Seg-Net) and a Transition network (Trans-Net). During inference, we only adopt the Seg-Net for segmentation.

#### 3.1 Formulation of the Point-Level Supervised Segmentation Problem

Given an input cell image set  $\{I_i\}_{i=1}^N$ , where  $N$  is the number of images in this set,  $I_i \in \mathbb{R}^{H \times W \times 3}$  with  $H, W$  representing the height and width of the image, respectively, and 3 being the number of channels of the image. Our goal is to obtain the mask of membranes ( $\tilde{M}_i \in \mathbb{R}^{H \times W \times 1}$ ) and nuclei ( $\tilde{S}_i \in \mathbb{R}^{H \times W \times 1}$ ), that is  $\{\tilde{M}_i, \tilde{S}_i\} = \sigma(\mathcal{F}_\theta(I_i))$ , where  $\mathcal{F}_\theta$  is a segmentation network (Seg-Net) and with trainable parameters  $\theta$ , and  $\sigma$  is the sigmoid activation function. We have point annotations  $P_i \in \mathbb{R}^{H \times W \times (c+1)}$  for image  $I_i$ , in which  $c$  is the number of semantic categories used to describe the states of membrane staining.

In order to train  $\mathcal{F}_\theta$  to segment membranes  $\tilde{M}_i$  and nuclei  $\tilde{S}_i$  using point annotations  $P_i$  in image  $I_i$ , we need to establish the relationship from input to segmentation, and

then to point annotation, as shown in Eq. (1) and Fig. 3.

$$I_i \xrightarrow{\mathcal{F}_\theta} \{\tilde{M}_i, \tilde{S}_i\} \xrightarrow{\mathcal{G}_\omega} \tilde{P}_i \sim= P_i, \quad (1)$$

where  $\mathcal{G}_\omega$  is the transition network (Tran-Net) with parameters  $\omega$ .  $\mathcal{G}_\omega$  transforms  $\{\tilde{M}_i, \tilde{S}_i\}$  to semantic points  $\tilde{P}_i \in \mathbb{R}^{H \times W \times (c+1)}$ , it should be noted that  $\tilde{M}_i$  and  $\tilde{S}_i$  respectively provide the semantic and spatial information to  $\mathcal{G}_\omega$  for semantic points prediction, so that the segmentation performance is crucial for  $\mathcal{G}_\omega$ . So that, by fitting  $\tilde{P}_i$  to  $P_i$  ( $\tilde{P}_i \sim= P_i$ ), the segmentation can be supervised.

### 3.2 Network Architecture

We adopt the U-Net [18] architecture for both  $\mathcal{F}_\theta$  and  $\mathcal{G}_\omega$  networks. The architecture of  $\mathcal{F}_\theta$  is conventional and follows the original U-Net [18]. However, in the decoder of  $\mathcal{G}_\omega$ , we replace the size of the last convolution kernel from  $1 \times 1$  to  $9 \times 9$ . This is because  $\mathcal{G}_\omega$  is utilized to predict the category of semantic points, which are the center points of cells and related to the membrane. Therefore, a larger receptive field is required for the convolution to improve the accuracy of category prediction. During inference, only  $\mathcal{F}_\theta$  is needed, and  $\mathcal{G}_\omega$  is discarded.

### 3.3 Decouple the Membranes and Nuclei Segmentation

Our goal is to use Seg-Net to generate masks for both membranes ( $\tilde{M}_i \in \mathbb{R}^{H \times W \times 1}$ ) and nuclei ( $\tilde{S}_i \in \mathbb{R}^{H \times W \times 1}$ ), i.e.,  $\{\tilde{M}_i, \tilde{S}_i\} = \sigma(\mathcal{F}_\theta(I_i))$ . However, the two Seg-Net channels are interdependent, which can result in nuclei and membranes being inseparably segmented. To overcome this issue, we enforce one channel to output the nuclei segmentation using a supervised mask  $S_i \in \mathbb{R}^{H \times W \times 1}$ . In this study, we create  $S_i$  by expanding each point annotation to a circle with a radius of 20. Thus, to provide semantic information to Tran-Net for predicting semantic points, the other channel must contain information describing the staining status of the membrane, which in turn decouples membrane segmentation.

Because both  $\tilde{S}_i$  and  $S_i$  are single-channel, we employ the naive  $L_1$  loss to supervise the segmentation of the nuclei, as shown in Eq. (2)

$$\ell_i^{\text{nuclei}} = |S_i - \tilde{S}_i|. \quad (2)$$

### 3.4 Constraints for Membranes Segmentation

As there are no annotations available for pixel-level membrane segmentation, the network could result in unwanted over-segmentation of membranes. This over-segmentation can take two forms: (1) segmentation of stained impurities, which can restrict the network's generalization performance by learning simple color features, and (2) segmentation of nuclei. To address these issues, we propose a normalization loss term,  $\ell_i^{\text{norm}}$ , which is an  $L_1$  normalization and is defined in Eq. (3). The purpose of this

loss term is to encourage the network to learn a smoother membrane segmentation that does not capture small stained regions or nuclei.

$$\ell_i^{\text{norm}} = \left\| \widetilde{M}_i \right\|_1. \quad (3)$$

However, relying solely on the  $\ell_i^{\text{norm}}$  normalization term might lead to a trivial solution, as it only minimizes the average value of the prediction result, potentially resulting in a minimal maximum confidence for the cell membrane segmentation (e.g., 0.03). To prevent this issue, we introduce a hinge-loss-like loss function, presented in Eq. (4), to constrain the distribution of membrane segmentation results. The hyper-parameter  $\tau$  in the hinge-loss function determines the expected value of the result, where a larger  $\tau$  corresponds to a smaller expected value. For instance, if  $\tau$  is set to 1 or 2, the expected values of the result would be 1 or 0.5, respectively. By selecting an appropriate value for  $\tau$ , we can mitigate the negative impact of  $\ell_i^{\text{norm}}$ .

$$\ell_i^{\text{hinge}} = \max(0, 1 - \tau \cdot \widetilde{M}_i). \quad (4)$$

### 3.5 Point-Level Supervision

Using  $\mathcal{G}_\omega$  to detect the central point of the cells is a typical semantic points detection task. The difference is that the input of  $\mathcal{G}_\omega$  is the output of  $\mathcal{F}_\theta$  rather than the image. Nevertheless, we can also employ the cross-entropy function for point-level supervision:

$$\ell_i^{\text{points}} = -\widetilde{P}_i \log(P_i). \quad (5)$$

To enhance the spatial supervision information of the point annotations  $P_i$ , it is worth noting that we extended each point annotation to a Gaussian circle with a radius of 5 pixels.

### 3.6 Total Loss

By leveraging the advantages of the above items, we can obtain the total loss as follows:

$$\mathcal{L}_i = \ell_i^{\text{nuclei}} + \ell_i^{\text{norm}} + \ell_i^{\text{hinge}} + \ell_i^{\text{points}}, \quad (6)$$

where  $\ell_i^{\text{norm}}$  and  $\ell_i^{\text{hinge}}$  are antagonistic, and their values are close to 0.5 in the ideal optimal state, which can be achieved at  $\tau = 1$  in  $\ell_i^{\text{hinge}}$ .

## 4 Experiments

In order to comprehensively verify the proposed method, we conduct extensive experiments on two IHC membrane-stained data sets, namely the PDL1 (Programmed cell depth 1 light 1) and HER2 (human epidermal growth factor receiver 2) datasets. The HER2 experiment is dedicated to validate segmentation performance, while the PDL1 experiment is utilized to verify the effectiveness of converting segmentation results into clinically relevant indicators.

## 4.1 Dataset

We collected 648 HER2 and 1076 PDL1 images at 40x magnification with a resolution of  $1024 \times 1024$  from WSIs. The PDL1 data only has point-level annotations, where pathologists categorize cells as positive or negative based on membrane staining. The HER2 data has both pixel-level and point-level annotations, where pathologists delineate the nuclei and membranes for pixel-level annotations and categorize cells based on membrane staining for point-level annotations. Pixel-level annotations are used for testing and fully supervised experiments only. We split the data into training and test sets in a 1:1 ratio and do not use a validation set since our method is trained without pixel-level annotations.

## 4.2 Implementation Details and Evaluation Metric

We totally train the networks 50 epochs and employ Adam optimizer [10] with the initial learning rate of  $5 \times 10^{-4}$  and the momentum of 0.9. Images are randomly cropped to  $512 \times 512$ , and data augmentations such as random rotation and flip were employed during model training. The hyper-parameter  $\tau$  in  $\ell_i^{\text{hinge}}$  is set to 1.0.

We employ the Intersection over Union (IoU) segmentation metric and pixel-level  $F_1$  score to validate the performance of the proposed method. However, only point-level annotations are equipped for the PDL1 dataset, we evaluate the segmentation performance at the point-level by converting the segmentation into key point predictions, and **the conversion process details are available in the supplementary materials.**

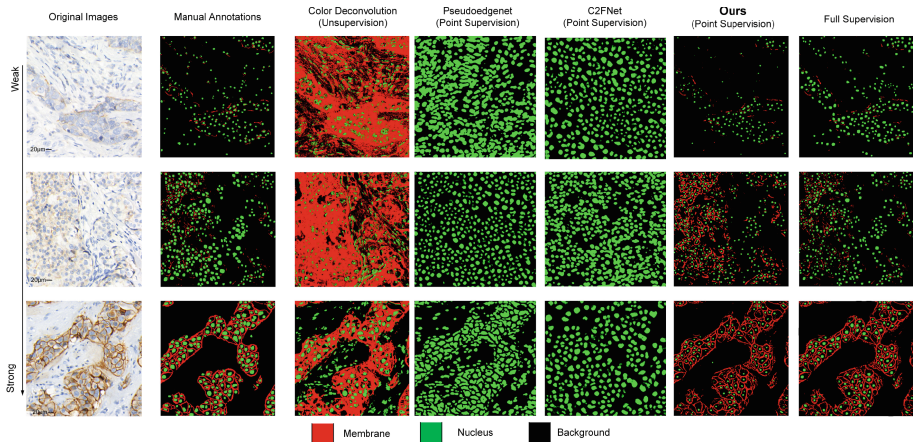
## 4.3 Result Analysis

**HER2 Results.** Table 1 shows the cell segmentation results of the proposed method and six comparison methods on the dataset HER2. Our proposed method can segment both cell nuclei and membranes simultaneously, outperforming both unsupervised methods and other point-level methods, with an IoU score of 0.5774 and an  $F_1$  score of 0.6899 for membranes, and an IoU score of 0.5242 and an  $F_1$  score of 0.6795 for nuclei. Furthermore, our ablation study shows that the hinge loss and normalization loss play important roles in improving the segmentation performance. Notably, other point-level methods not only fail to segment the cell membranes but also have limited performance in segmenting cell nuclei due to over-segmentation and under-segmentation errors, as shown in Fig. 4.

**PDL1 Results.** We chose to compare our method with unsupervised segmentation methods because existing point-supervised segmentation methods are unable to segment cell membranes. We present their results in Table 2, which illustrates that the proposed method outperforms other methods, achieving  $F_1$  scores of 0.7131 and 0.7064 for negative and positive-stained cells, respectively. Among the unsupervised methods, color deconvolution [4] shows the best performance with  $F_1$  scores of 0.5984 and 0.6136 for negative and positive cells, respectively. However, our proposed method significantly outperformed it. Besides, qualitative experimental results can be found in the supplementary materials.

**Table 1.** Comparison of the cell segmentation results on HER2 test data. w/o: without.

Supervised Settings	Methods	Membranes		Nuclei	
		IoU	$F_1$ score	IoU	$F_1$ score
Unsupervised	USAR (our implementation) [6]	0.0865	0.1356	0.0832	0.1165
	Watershed [17]	0.3561	0.4427	0.0721	0.1285
	Active Contour [25]	0.3331	0.3938	0.0973	0.1571
	Color Deconvolution [4]	0.4242	0.5148	0.1418	0.2455
Point-level Supervised	C2FNet [21]	/	/	0.3007	0.4044
	Pseudoedgenet [27]	/	/	0.1548	0.2663
	Ours w/o hinge and norm loss	0.4877	0.5001	<b>0.5656</b>	<b>0.7155</b>
	Ours w/o hinge loss	0	0	0.5357	0.6908
	Ours	<b>0.5774</b>	<b>0.6899</b>	0.5242	0.6795
Fully supervised	Fully supervised	0.7096	0.8068	0.6873	0.7648

**Fig. 4.** Qualitative results on the HER2 test set.**Table 2.** Comparison Point-level Results of the PDL1 Test Dataset.

Methods	Negative-stained Cells			Positive-stained Cells		
	Recall	Precision	$F_1$ score	Recall	Precision	$F_1$ score
Watershed [17]	0.6601	0.5597	0.5117	0.5650	0.5272	0.4853
Active Contour [25]	0.5876	0.5259	0.4956	0.5785	0.5266	0.4713
Color Deconvolution [4]	0.6583	0.5715	0.5984	0.7161	0.5758	0.6136
Ours	<b>0.7044</b>	<b>0.7791</b>	<b>0.7131</b>	<b>0.7308</b>	<b>0.6970</b>	<b>0.7064</b>

## 5 Conclusion

In this paper, we present a novel method for precise segmentation of cell membranes and nuclei in immunohistochemical (IHC) membrane staining images using only point-level

supervision. Our method achieves comparable performance to fully supervised pixel-level annotation methods while significantly reducing annotation costs, only requiring one-tenth of the cost of pixel-level annotation. This approach effectively reduces the expenses involved in developing, deploying, and adapting IHC membrane-stained image analysis algorithms. In the future, we plan to further optimize the segmentation results of cell nuclei to further boost the performance of the proposed method, and extend it to the whole slide images (WSIs).

**Acknowledgements.** This work is supported by the National Natural Science Foundation of China (NSFC Grant No. 62073260, No.62106198 and No.62276052), and the Natural Science Foundation of Shaanxi Province of China (2021JQ-461), the General Project of Education Department of Shaanxi Provincial Government under Grant 21JK0927. Medical writing support is provided by AstraZeneca China. The technical and equipment support is provided by HangZhou DiYingJia Technology Co., Ltd (DeepInformatics++). The authors would like to thank the medical team at AstraZeneca China and technical team at DeepInformatics++ for their scientific comments on this study.

## References

1. Aurenhammer, F., Klein, R.: Voronoi diagrams. *Handb. Comput. Geom.* **5**(10), 201–290 (2000)
2. Di Cataldo, S., Ficarra, E., Macii, E.: Selection of tumor areas and segmentation of nuclear membranes in tissue confocal images: a fully automated approach. In: 2007 IEEE International Conference on Bioinformatics and Biomedicine (BIBM 2007), pp. 390–398. IEEE (2007)
3. Elmoataz, A., Schüpp, S., Clouard, R., Herlin, P., Bloyet, D.: Using active contours and mathematical morphology tools for quantification of immunohistochemical images. *Signal Process.* **71**(2), 215–226 (1998)
4. Ficarra, E., Di Cataldo, S., Acquaviva, A., Macii, E.: Automated segmentation of cells with ihc membrane staining. *IEEE Trans. Biomed. Eng.* **58**(5), 1421–1429 (2011)
5. Graham, S., et al.: Hover-net: simultaneous segmentation and classification of nuclei in multi-tissue histology images. *Med. Image Anal.* **58**, 101563 (2019)
6. Han, L., Yin, Z.: Unsupervised network learning for cell segmentation. In: de Bruijne, M., et al. (eds.) MICCAI 2021. LNCS, vol. 12901, pp. 282–292. Springer, Cham (2021). [https://doi.org/10.1007/978-3-030-87193-2\\_27](https://doi.org/10.1007/978-3-030-87193-2_27)
7. Hou, L., Agarwal, A., Samaras, D., Kunc, T.M., Gupta, R.R., Saltz, J.H.: Robust histopathology image analysis: to label or to synthesize? In: Proceedings of the IEEE/CVF Conference on Computer Vision and Pattern Recognition, pp. 8533–8542 (2019)
8. Ji, Y., et al.: Multi-compound transformer for accurate biomedical image segmentation. In: de Bruijne, M., et al. (eds.) MICCAI 2021. LNCS, vol. 12901, pp. 326–336. Springer, Cham (2021). [https://doi.org/10.1007/978-3-030-87193-2\\_31](https://doi.org/10.1007/978-3-030-87193-2_31)
9. Khamehneh, F.D., Razavi, S., Kamasak, M.: Automated segmentation of cell membranes to evaluate her2 status in whole slide images using a modified deep learning network. *Comput. Biol. Med.* **110**, 164–174 (2019)
10. Kingma, D.P., Ba, J.: Adam: a method for stochastic optimization. arXiv preprint [arXiv:1412.6980](https://arxiv.org/abs/1412.6980) (2014)
11. Lin, A., Chen, B., Xu, J., Zhang, Z., Lu, G., Zhang, D.: Ds-transunet: dual swin transformer u-net for medical image segmentation. *IEEE Trans. Instrument. Meas.* **71**, 1–15 (2022)

12. Luna, M., Kwon, M., Park, S.H.: Precise separation of adjacent nuclei using a siamese neural network. In: Shen, D., et al. (eds.) MICCAI 2019. LNCS, vol. 11764, pp. 577–585. Springer, Cham (2019). [https://doi.org/10.1007/978-3-030-32239-7\\_64](https://doi.org/10.1007/978-3-030-32239-7_64)
13. Bueno-de Mesquita, J.M., Nuyten, D., Wesseling, J., van Tinteren, H., Linn, S., van De Vijver, M.: The impact of inter-observer variation in pathological assessment of node-negative breast cancer on clinical risk assessment and patient selection for adjuvant systemic treatment. *Ann. Oncol.* **21**(1), 40–47 (2010)
14. Mi, H., et al.: A quantitative analysis platform for pd-l1 immunohistochemistry based on point-level supervision model. In: IJCAI, pp. 6554–6556 (2019)
15. Qaiser, T., Rajpoot, N.M.: Learning where to see: a novel attention model for automated immunohistochemical scoring. *IEEE Trans. Med. Imaging* **38**(11), 2620–2631 (2019)
16. Qu, H., et al.: Weakly supervised deep nuclei segmentation using points annotation in histopathology images. In: International Conference on Medical Imaging with Deep Learning, pp. 390–400. PMLR (2019)
17. Roerdink, J.B., Meijster, A.: The watershed transform: definitions, algorithms and parallelization strategies. *Fundamenta informaticae* **41**(1–2), 187–228 (2000)
18. Ronneberger, O., Fischer, P., Brox, T.: U-Net: convolutional networks for biomedical image segmentation. In: Navab, N., Hornegger, J., Wells, W.M., Frangi, A.F. (eds.) MICCAI 2015. LNCS, vol. 9351, pp. 234–241. Springer, Cham (2015). [https://doi.org/10.1007/978-3-319-24574-4\\_28](https://doi.org/10.1007/978-3-319-24574-4_28)
19. Saha, M., Chakraborty, C.: Her2net: a deep framework for semantic segmentation and classification of cell membranes and nuclei in breast cancer evaluation. *IEEE Trans. Image Process.* **27**(5), 2189–2200 (2018)
20. Swiderska-Chadaj, Z., et al.: Learning to detect lymphocytes in immunohistochemistry with deep learning. *Med. Image Anal.* **58**, 101547 (2019)
21. Tian, K., et al.: Weakly-supervised nucleus segmentation based on point annotations: a coarse-to-fine self-stimulated learning strategy. In: Martel, A.L., et al. (eds.) MICCAI 2020. LNCS, vol. 12265, pp. 299–308. Springer, Cham (2020). [https://doi.org/10.1007/978-3-030-59722-1\\_29](https://doi.org/10.1007/978-3-030-59722-1_29)
22. Vogel, C., et al.: PI-07-02: discordance between central and local laboratory her2 testing from a large her2- negative population in virgo, a metastatic breast cancer registry (2011)
23. Wolff, A.C., et al.: Human epidermal growth factor receptor 2 testing in breast cancer: American society of clinical oncology/college of american pathologists clinical practice guideline focused update. *Arch. Pathol. Lab. Med.* **142**(11), 1364–1382 (2018)
24. Xu, J., et al.: Stacked sparse autoencoder (ssae) for nuclei detection on breast cancer histopathology images. *IEEE Trans. Med. Imaging* **35**(1), 119–130 (2015)
25. Yang, L., Meer, P., Foran, D.J.: Unsupervised segmentation based on robust estimation and color active contour models. *IEEE Trans. Inf. Technol. Biomed.* **9**(3), 475–486 (2005)
26. Yang, X., Li, H., Zhou, X.: Nuclei segmentation using marker-controlled watershed, tracking using mean-shift, and kalman filter in time-lapse microscopy. *IEEE Trans. Circ. Syst. I: Regul. Papers* **53**(11), 2405–2414 (2006)
27. Yoo, I., Yoo, D., Paeng, K.: PseudoEdgeNet: nuclei segmentation only with point annotations. In: Shen, D., et al. (eds.) MICCAI 2019. LNCS, vol. 11764, pp. 731–739. Springer, Cham (2019). [https://doi.org/10.1007/978-3-030-32239-7\\_81](https://doi.org/10.1007/978-3-030-32239-7_81)